

## Losses in luminescent solar concentrators unveiled



C. Tummelshammer, A. Taylor, A.J. Kenyon, I. Papakonstantinou\*

Department of Electronic and Electrical Engineering, University College London, London WC1E 7JE, United Kingdom

### ARTICLE INFO

#### Article history:

Received 11 May 2015

Received in revised form

6 August 2015

Accepted 11 August 2015

Available online 5 September 2015

#### Keywords:

Luminescent solar concentrator

Integrating sphere

Optical efficiency

Loss channels

Quantum yield

### ABSTRACT

A novel experimental method is presented to determine the optical efficiency and the loss channels of a luminescent solar concentrator (LSC). Despite strong promise, LSCs have not yet reached their full potential due to various mechanisms affecting the device's optical efficiency. Among those loss channels, escape cone and non-unity quantum yield losses are generally the most dominant. To further advance the field of LSCs, it is vital to understand the impact of each independently. So far, researchers have only characterized the total loss in LSCs. Here, an experimental method is proposed to separate the contribution from each individual loss channel. The experimental apparatus is the same as used for quantum yield measurements of fluorophores in solid samples. Therefore, the setup is commonly available to research groups already involved in LSC research. The accuracy of this method is demonstrated by comparing the experimental results with Monte-Carlo ray tracing. Our experimental method can have a strong impact on LSC research as it offers a means to unveil the loss channels of LSCs in addition to the optical efficiency.

© 2015 The Authors. Published by Elsevier B.V. This is an open access article under the CC BY license (<http://creativecommons.org/licenses/by/4.0/>).

### 1. Introduction

Luminescent solar concentrators (LSCs) offer an encouraging means to include solar energy to the built environment; they concentrate sunlight without the need for expensive tracking equipment and their design makes them suitable as windows. LSCs are composed of a transparent matrix material, generally a slab of poly(methyl methacrylate) (PMMA), which is doped with fluorophores to absorb the incoming sunlight. The absorbed energy is then emitted at a longer wavelength and, given the emission falls outside of the escape cone, trapped through total internal reflection within the slab of PMMA. Light that is guided towards the sides of the slab is converted into electricity by solar cells. The share of photons concentrated towards the sides of the LSC is denoted the optical efficiency of the device.

Though invented in the late 70s [1,2], LSCs still exhibit limited efficiencies mainly due to two loss channels: (1) photons emitted by a fluorophore within the *escape cone* and lost through the front and back surfaces of the LSC, and (2) photons absorbed by a fluorophore and lost due to a *non-unity quantum yield*. Both loss channels are further aggravated by re-absorption which is due to the overlap of the absorption and emission spectra of the fluorophore. Additionally, fluorophores such as organic dye molecules often have a narrow absorption band which results in a large share

of the solar spectrum not being absorbed at all. To enhance the efficiency of LSCs, it is crucial to determine which loss channel deteriorates the performance of the LSC. While the wavelength band absorbed by the fluorophore can be determined with absorption measurements, it is less straightforward to experimentally investigate the extent to which escape cone and quantum yield losses degrade the performance of the LSC.

Different methods have been proposed to experimentally measure the optical efficiency of a LSC. The side surface emission of a LSC can be collected via an aperture in an integrating sphere while the illuminated front surface remains outside the integrating sphere [3–7]. If the whole sample is placed within the integrating sphere, one can determine the optical efficiency by selectively blocking the side surface emission using a black tape or marker [8–13]. Side surface emissions can also be measured using a fiber with a cosine corrector as a probe that is held against the respective side surface [14]. However, none of these proposed methods reveal the fate of the lost photons; whether they are lost due to a non-unity quantum yield or escape cone losses. In this work we present, to the best of our knowledge, for the very first time a method to experimentally determine and distinguish these two important loss channels for LSCs. This will allow researchers to better understand the limitations of their designs and to more effectively improve LSC efficiency for building-integrated photovoltaics.

Bragg mirrors or aligned fluorophores are means to enhance the trapping efficiency within a LSC [15–17]. Our method can determine the reduction in escape cone losses achieved by such a

\* Corresponding author. Tel.: +44 20 7679 7302.

E-mail address: [i.papakonstantinou@ucl.ac.uk](mailto:i.papakonstantinou@ucl.ac.uk) (I. Papakonstantinou).

prototype LSC. It was also proposed to link and align different fluorophores to enhance the trapping efficiency and separate the absorption and emission process [6,17–19]. In addition to quantifying the reduction in escape cone losses, our method is also able to measure the potential change in non-unity quantum yield losses; the linking of fluorophores could deteriorate or even improve the quantum yield of the involved fluorophores. Previous methods are only able to determine the total loss which in some cases

remains constant, e.g. when the reduction in escape cone losses and the change in non-unity quantum yield losses cancel each other out.

The photon paths within a LSC, which our experimental method is able to distinguish between, are shown in Fig. 1(a). An incoming photon is either reflected off the top surface, not dye absorbed, or absorbed by a fluorophore. After the initial absorption, the photon is either concentrated to the side surfaces, lost via the escape cone, or lost due to a non-unity quantum yield. LSCs fabricated for this study are doped with four different dye molecules which are shown in Fig. 1(b). Optical measurements are compared to Monte-Carlo ray tracing simulations which show very good agreement.

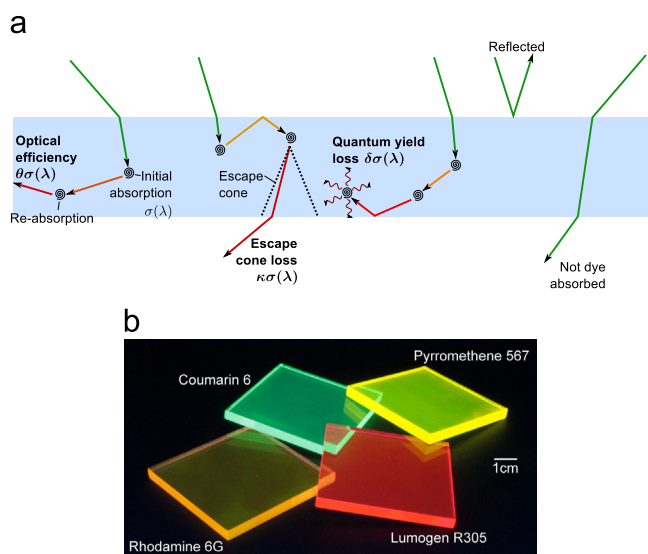


**Fig. 1.** (a) Fate of photons our experimental model is able to distinguish. After the initial absorption, a photon is either concentrated to a side surface with probability  $\theta$ , lost via the escape cone with probability  $\kappa$ , or lost due to a non-unity quantum yield with probability  $\delta$ . To take into account the initial absorption, the three probabilities have to be multiplied with  $\sigma(\lambda)$ , the probability that an incoming photon is absorbed. (b) LSCs doped with different dye molecules under UV illumination. The LSCs at the front are doped with Rhodamine 6G (left) and Lumogen R305 (right) and at the back with Coumarin 6 (left) and Pyromethene 567 (right).

## 2. Theory

In this section, the theoretical background and the experimental setup of our novel experimental method to determine the efficiency and loss channels of a LSC are presented. The experimental method is based on the most common approach to determine the quantum yield of fluorophores incorporated in solid samples such as a slab of PMMA [20]. A monochromatic light source illuminates an integrating sphere that is connected to a spectrometer via a fiber cable. As shown in Fig. 2, five different configurations are necessary of which the first three are the same as used for quantum yield measurements [20].

In the first configuration (I) no LSC sits within the integrating sphere and only the incoming monochromatic light source is measured. For the second configuration (II) the LSC is placed within the integrating sphere and the incoming beam misses the LSC initially; thus only light scattered off the surface of the integrating sphere is absorbed by the LSC. The third configuration (III) is similar to the second one but the incoming beam now directly impinges on the LSC. For the remaining two configurations, (IV) and (V), the side surfaces of the LSC are blackened with a black

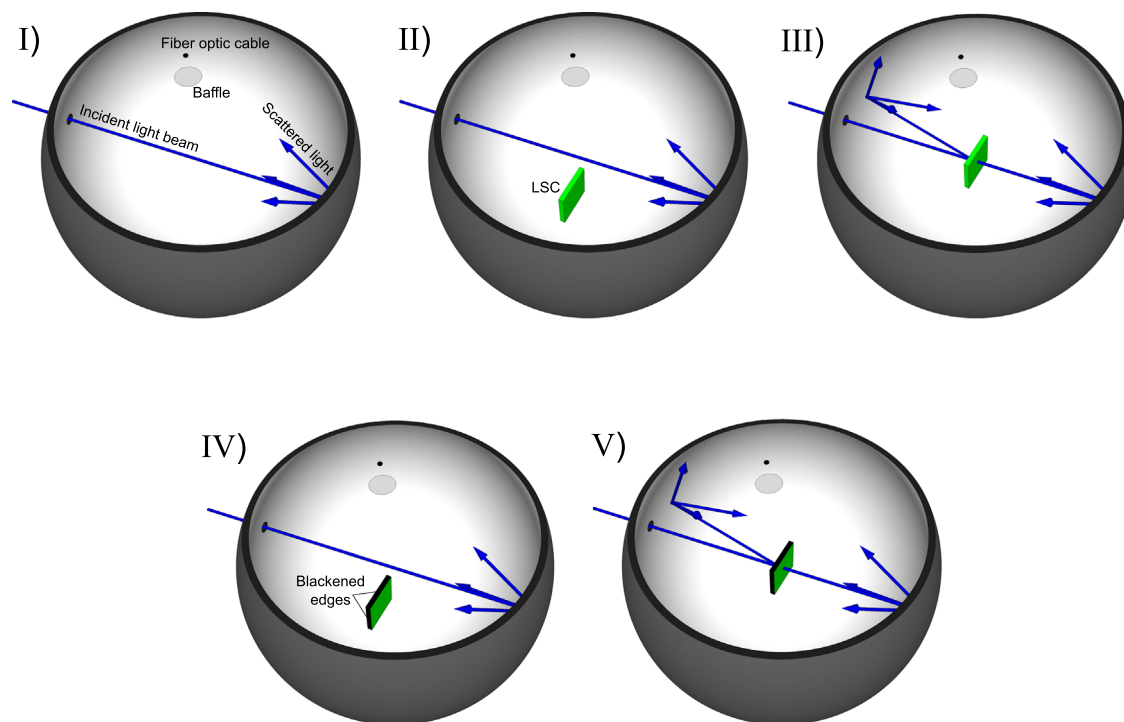


**Fig. 2.** The five configurations necessary to determine the internal optical efficiency and loss channels of a LSC: (I) the integrating sphere is empty; (II) the LSC is placed inside the sphere but not in the incident beam path; (III) the incident light beam directly impinges on the LSC; (IV) same as configuration (II) but the side surfaces are blackened; (V) same as configuration (III) but the side surfaces are blackened.

marker to avoid transmission and total internal reflection. Otherwise the configurations in (IV) and (V) are the same as in (II) and (III) respectively. The black marker used prevents transmission and total internal reflection by at least 99% over the wavelength range of interest (see Supplementary Material).

In each configuration the integrated photon fluxes (the areas under the measured spectra) of the unabsorbed incoming beam and the emitted light are denoted  $L$  and  $P$ , respectively. The quantum yield of a fluorophore is given by the number of emitted photons divided by the number of absorbed photons. Similarly, the optical efficiency of a LSC is the number of photons reaching the side surfaces divided by the number of photons incident on the LSC. Therefore, the integrating sphere setup has to be calibrated so that the measured spectra are proportional to photon counts.

Once a photon is absorbed within the LSC, there are three possible outcomes (see also Fig. 1(a)): (1) the photon reaches the side surfaces with probability  $\theta$ , (2) the photon is lost via the escape cone through the front and back surfaces with probability  $\kappa$ , or (3) the photon is lost due to a non-unity quantum yield with probability  $\delta$ . Additionally, we differentiate between photons absorbed from the incoming beam before it is scattered off the integrating sphere surface (subscript  $i$ ) and absorbed photons that were scattered off the integrating sphere surface first (subscript  $s$ ). Thus  $\theta_i$  is the probability that a photon absorbed from the initial incoming light beam will reach one of the side surfaces of the LSC.

The probability  $\theta$  can be denoted the *internal optical efficiency* as it only considers absorbed photons, while the *optical efficiency* of an LSC compares the number of photons reaching the side surfaces to all photons impinging on the front surface of the LSC. Using the internal optical efficiency has the advantage that it is independent of the incoming light beam's wavelength which will be shown in Section 4. This independence is a consequence of both Kasha's and the Kasha–Vavilov rules which state that the emission spectrum and the quantum yield are generally independent of the excitation wavelength [21].

Our experimental method does also take into account host absorption. The probability  $\delta$  includes not only non-unity quantum yield losses but also host absorption losses. However, the number of photons lost due to host absorption is generally very small compared to the number of photons lost due to a non-unity quantum yield (see Supplementary Material). For all investigated LSC designs, host absorption accounts for less than 1% of all absorbed photons. For larger LSCs host absorption losses will increase but so will non-unity quantum yield losses. Therefore,  $\delta$  will generally be mostly comprised of non-unity quantum yield losses.

There exist two different, though related, methods to determine the quantum yield of a fluorophore in solid samples using an integrating sphere [20,22]. Both can be used to derive the equations that will determine  $\theta$ ,  $\kappa$  and  $\delta$ . The first one, the *standard method*, is the most common method to measure the quantum yield of a fluorophore and requires configurations (I), (II), and (III) [20]. A more recent method, the *simplified* one, only requires configurations (I) and (III) to measure the quantum yield of a fluorophore [22]. With the help of configurations (IV) and (V) our novel experimental method can additionally determine the internal optical efficiency and loss channels of a LSC which will be shown in the following two sections.

### 2.1. Standard method

In configurations (III) and (V) the incoming light beam first impinges on the LSC. Let  $A = 1 - L_{III}/L_I$  be the share of the incoming light beam that is absorbed by the LSC [20]. The remaining unabsorbed incoming light beam will be scattered off the integrating sphere surface and be absorbed by the LSC with

probability  $\mu = 1 - L_{II}/L_I$  [20]. Then the integrated LSC emissions for configurations (II) to (V) are given by

$$\begin{aligned} P_{II} &= L_I \mu (\theta_s + \kappa_s) \\ P_{III} &= L_I A (\theta_i + \kappa_i) + (1 - A) L_I \mu (\theta_s + \kappa_s) \\ P_{IV} &= L_I \mu \kappa_s \\ P_V &= L_I A \kappa_i + (1 - A) L_I \mu \kappa_s \end{aligned} \quad (1)$$

For configuration (III), the first part on the right-hand side corresponds to the light absorbed from the incoming light beam while the second part corresponds to the scattered light that is absorbed. In configurations (II) and (IV) the incoming light beam misses the LSC and thus only scattered light is absorbed by the LSC. As the side surfaces are blackened out in configurations (IV) and (V), only the escape cone losses through the front and back surfaces ( $\kappa$ ) contribute to the spectra.

By assuming that the position where the light is scattered off the integrating sphere surface is not crucial, one can write the measured spectrum due to absorbed scattered light in configurations (III) and (V) as follows [20]:

$$\begin{aligned} \text{(III)} \quad &(1 - A)(L_{II} + P_{II}) \\ \text{(V)} \quad &(1 - A)(L_{IV} + P_{IV}) \end{aligned} \quad (2)$$

Combining Eqs. (1) and (2) yields the following results for  $\theta_i$  and  $\kappa_i$ :

$$\theta_i + \kappa_i = \frac{P_{III} - (1 - A)P_{II}}{L_I A} \quad (3)$$

$$\kappa_i = \frac{P_V - (1 - A)P_{IV}}{L_I A} \quad (4)$$

The probability that a photon is lost due to a non-unity quantum yield can be determined by considering that  $\theta_i + \kappa_i + \delta_i = 1$ . Eqs. (3) and (4) are the main results of this work as they determine the internal optical efficiency, the escape cone losses and the non-unity quantum yield losses of the LSC investigated. This work is the first to present a single method that can determine the efficiency and loss channels of a LSC. Eq. (3) is equal to the formula that determines the quantum yield of the fluorophore [20]:

$$\eta = \frac{P_{III} - (1 - A)P_{II}}{L_I A} \quad (5)$$

This is intuitive as the probability of light lost via the escape cone through the front and back surfaces combined with the probability of light being emitted through the side surfaces as a function of absorbed photons is equal to the quantum yield of the fluorophore (assuming neglectable re-absorption).

Re-absorption of emitted photons can falsify the quantum yield calculation in Eq. (5) though; the re-absorption can be taken into account by comparing the observed emission spectrum with the spectrum of a single emission event [23]. This is not necessary for Eqs. (3) and (4) as re-absorption and subsequent escape cone and non-unity quantum yield losses are, unfortunately, part of a LSC performance metric. Second order re-absorption (emitted photons that escape from the LSC, reflect off the integrating sphere and are absorbed again by the LSC) could potentially amend the results; however, as shown in the Supplementary Material, the error is less than 0.5% for the investigated LSCs.

### 2.2. Simplified method

The standard method uses 3 configurations to measure the quantum yield [20]. However, as shown recently, only two configurations – (I) and (III) – are necessary to determine the quantum yield of a fluorophore using an integrating sphere [22]. Similarly, it

is sufficient to use configurations (I), (III) and (V) to determine the internal optical efficiency and loss channels of the LSC. The simplified quantum yield measurement technique was presented using a theoretical framework elsewhere [22]. We extend this framework to derive formulas for the LSC metrics. Moreover, we experimentally validate this simplified quantum yield measurement technique by comparing it to the standard quantum yield measurement technique.

The total absorption (absorption of the incoming beam and the scattered light) in configuration (III) is given by  $B = 1 - L_{III}/L_I$ . Then the quantum yield of the fluorophore  $\eta_N$ , the internal optical efficiency  $\theta_N$  and the escape cone losses  $\kappa_N$  can be written as

$$\eta_N = \theta_N + \kappa_N = \frac{P_{III}}{L_I B} \quad (6)$$

$$\kappa_N = \frac{P_V}{L_I B} \quad (7)$$

Eqs. (6) and (7) form part of our experimental method and are equivalent to Eqs. (3) and (4), respectively. In contrast to the standard method only three instead of five configurations are necessary. With either method, the optical efficiency and loss channels of a LSC can be determined.

This simplified method is particularly useful for low light levels which can be due to either a low concentration or a low quantum yield of the fluorophore. In both cases the measured emission spectra in configurations (II) and (IV) can be quite low and thus be dominated by noise which can cause the derived quantum yield to be erroneous. If the sample does not suffer from low light levels, the standard and simplified methods agree very well though which will be shown below. However, if this simplified approach is applied, one cannot distinguish between the response of the LSC to the incoming light beam and the scattered light. This has little impact though, as the absorption of the incoming light beam accounts for the majority of the total absorbed power.

### 2.3. Optical efficiency

Once the internal optical efficiency  $\theta$  has been determined, the optical efficiency  $\eta_{opt}$  of a LSC can be calculated. The optical efficiency is equal to the number of photons reaching the side surfaces divided by the number of photons impinging on the front surface of the LSC. Thus, it also takes into account reflections at the front surface and photons that are not absorbed by the fluorophores. The internal optical efficiency  $\theta$  denotes the probability of a photon reaching a side surface after a photon of the incoming beam has been absorbed. Thus, the internal optical efficiency just has to be multiplied with the probability that a photon of the incoming light beam is absorbed within the LSC. This will yield the optical efficiency which is given by

$$\eta_{opt}(\lambda) = \theta\sigma(\lambda) \quad (8)$$

where  $\sigma(\lambda)$  is the share of incoming light that is absorbed by the LSC at wavelength  $\lambda$ . The probability of absorption is dependent on wavelength as it is a function of the absorption cross section of the fluorophore. The probability of absorption can be determined using an absorbance measurement of the LSC. Similar to Eq. (8), the escape cone and non-unity quantum yield losses relative to all incident photons can be calculated as well. To recap, the optical efficiency and the loss channels of a LSC with their respective probabilities are depicted in Fig. 1(a).

## 3. Experimental section

### 3.1. Materials

Methyl methacrylate (MMA, Sigma Aldrich) and 2, 2' - Azobis(2-methylpropionitrile) (AIBN, Sigma Aldrich) are used as monomer and radical initiator respectively. Poly(methyl methacrylate) (PMMA) was supplied by Lucite. Coumarin 6 and Rhodamine 6G were purchased from Sigma Aldrich, while Pyrromethene 567 was acquired from Exciton. Lumogen R305 was made available by BASF.

### 3.2. LSC device fabrication

First, the desired quantity of dye molecules is dissolved in MMA using a magnetic stirrer. Then the solution is heated to 60 °C and the PMMA is added at a 9:1 (MMA:PMMA) weight ratio. Once the PMMA is dissolved, the solution is quenched and 0.8 wt% of AIBN is added. Subsequently, the mixture is poured into a mold which is placed in a water bath at 60 °C for 18 h. To post-cure the sample, it is put into the oven at 80 °C for 2 h and at 100 °C, 110 °C, and 120 °C for 1 h each. Samples are cut to size using a laser cutter (Universal Laser Systems) and the side surfaces are polished.

### 3.3. Optical characterization

The absorbance measurements of the doped LSCs are performed using a UV-vis spectrophotometer (Shimadzu). A second UV-vis spectrophotometer (PerkinElmer) was used to measure the reflection and transmission of undoped LSCs. To determine the emission profile of the different dye molecules in PMMA, low concentration samples (Coumarin 6:  $4 \times 10^{-7}$  mol L<sup>-1</sup>, Lumogen R305: 1 ppm, Rhodamine 6G:  $6.5 \times 10^{-7}$  mol L<sup>-1</sup>, and Pyrromethene 567:  $8 \times 10^{-7}$  mol L<sup>-1</sup>) are used to avoid re-absorption. The emission measurements were taken using a fluorescence spectrometer (Edinburgh Instruments). The equipment used to measure the quantum yield and the internal optical efficiency is shown in Fig. 2. The integrating sphere (Mulsphere) is illuminated by a 100 W quartz tungsten halogen lamp (Oriel Instruments) that is connected to a monochromator (Oriel Instruments). Light is coupled from the monochromator to a fiber cable and collimated into the integrating sphere with the help of a collimating lens (Ocean Optics). A fiber cable connects the integrating sphere to a CCD spectrometer (Ocean Optics). Our integrating sphere has a diameter of 50 cm and thus would be able to accommodate most LSCs fabricated for research purposes [3–14,24].

## 4. Results and discussion

In this section we present our experimental results and compare them to Monte-Carlo ray tracing, a simulation method already previously used to model LSCs [25,17]. Table 1 shows the different LSC designs investigated in this work and their measured quantum yields. To take into account re-absorption and its impact on the measured quantum yield, the emission profile of one single emission event is compared to the measured emission profile [23]. All LSCs have a size of  $60 \times 60 \times 5$  mm<sup>3</sup>. The LSCs were fabricated using methyl methacrylate (MMA) as monomer and a standard water-bath method which is outlined in Section 3. For each LSC three independent quantum yield and internal optical efficiency measurements were performed.

The quantum yield of Lumogen R305 is measured to be around 95% which closely matches previous findings [24,26,27]. The quantum yield only shows a weak dependence on concentration

**Table 1**  
Investigated LSC designs with their respective fluorophore concentrations and measured quantum yields. The experimental quantum yield measurements are shown using both the standard and the simplified method. The quantum yields used for the ray tracing simulations are reported as well.

Dye	Concentration	Quantum yield (%)		
		Standard method	Simplified method	Ray tracing
Coumarin 6	$1.0 \times 10^{-5} \text{ mol L}^{-1}$	100.3 + / - 1.5	99.4 + / - 0.9	99.4
	$1.0 \times 10^{-4} \text{ mol L}^{-1}$	99.2 + / - 0.8	99.1 + / - 0.8	99.2
	$1.0 \times 10^{-3} \text{ mol L}^{-1}$	97.9 + / - 0.4	97.8 + / - 0.4	97.9
Lumogen R305	10 ppm <sup>a</sup>	97.2 + / - 0.5	96.2 + / - 0.2	96.2
	40 ppm <sup>a</sup>	95.5 + / - 0.2	95.4 + / - 0.2	95.5
	60 ppm <sup>a</sup>	95.6 + / - 0.2	95.5 + / - 0.3	95.5
	150 ppm <sup>a</sup>	94.4 + / - 0.2	94.4 + / - 0.2	94.4
Rhodamine 6G	$5.5 \times 10^{-6} \text{ mol L}^{-1}$	72.5 + / - 0.6	76.3 + / - 0.2	76.3
	$1.0 \times 10^{-5} \text{ mol L}^{-1}$	71.7 + / - 0.2	74.2 + / - 0.2	74.2
Pyrromethene 567	$1.0 \times 10^{-5} \text{ mol L}^{-1}$	95.1 + / - 0.2	96.0 + / - 0.1	96.0
	$1.0 \times 10^{-4} \text{ mol L}^{-1}$	94.2 + / - 0.1	94.2 + / - 0.1	94.2
	$1.0 \times 10^{-3} \text{ mol L}^{-1}$	92.8 + / - 0.1	92.8 + / - 0.1	92.8

<sup>a</sup> BASF does not disclose the molecular weight of Lumogen R305.

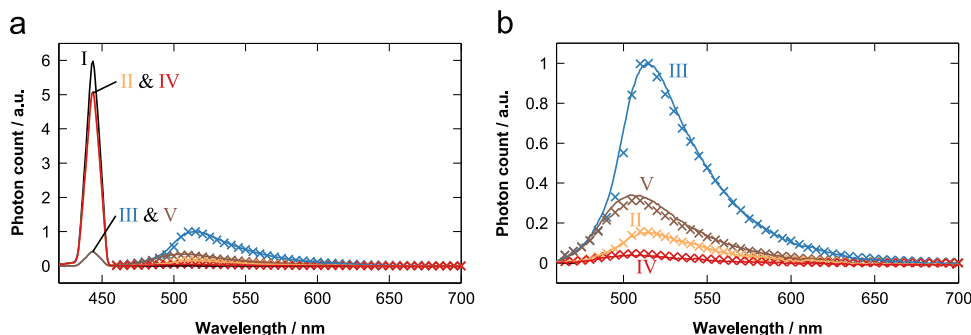


**Fig. 3.** Comparison between experimental measurements (solid lines) and ray tracing (crosses) as a function of wavelength for the LSC doped with Coumarin 6 at a concentration of  $10^{-4} \text{ mol L}^{-1}$ . Both plots show the same spectral data with (a) depicting the signal from the excitation source and the LSC emission and (b) focusing on the LSC emission only. Configuration (I) is black, (II) is orange, (III) is blue, (IV) is red, and (V) is brown. For the ray tracing simulations the LSC was excited by a single wavelength and only the emission from the LSC is shown. Ray tracing and experimental measurements were normalized with a constant so that the maximum values of spectra (III) are equal to unity. (For interpretation of the references to color in this figure caption, the reader is referred to the web version of this paper.)

and the measurements agree well for both methods. For Rhodamine 6G the quantum yield measurements vary between 71% and 76% depending on the concentration and the method. This range agrees very well with earlier work at the concentrations investigated [28]. Rhodamine 6G measurements are only available at low concentrations as the dye has a low solubility in MMA. At these low concentrations the measured signal strength of the dye emission inside the integrating sphere is low and thus more prone to be noisy. As a result, the two methods do not agree as well as for the other dye molecules. Coumarin 6 demonstrates the highest quantum yield among all measured dyes. A near-unity quantum yield is found which shows only a slight dependence on concentration. This is higher than the often reported quantum yield of 78% for Coumarin 6 in ethanol [29]. However, it was found that Coumarin 6 – and other Coumarin dyes – show a higher quantum yield within a rigid matrix such as PMMA which is confirmed by our measurements [30,31]. Pyrromethene 567 also has a very high quantum yield of around 95% which is in the range of previous quantum yield measurements in different solvents [32]. Similar to Coumarin 6 and Lumogen R305, the quantum yield of Pyrromethene 567 decreases only marginally with increasing concentration. Table 1 also shows the quantum yields adapted for the ray tracing simulations. For most LSCs it would make no difference if we would use the quantum yield measured using the standard or the simplified method as they match so closely. Only for low concentrations both methods disagree slightly. In such a case we chose to use the simplified method's result as it does not take into

account configurations (II) and (IV) which could potentially have a low signal-to-noise ratio at low concentrations.

Fig. 3 shows the spectral output of all five configurations for the LSC doped with Coumarin 6 at a concentration of  $10^{-4} \text{ mol L}^{-1}$ . The experimental measurements and ray tracing results are in very good agreement; in both cases the peak emission wavelength in configuration (III) is red-shifted by 10 nm compared to configuration (V). Photons emitted through the side surfaces of the LSC have to travel longer distances through the LSC compared to the front and back surfaces. As a result, they are more likely to be re-absorbed and red-shifted. In configuration (V) photons concentrated to the side surfaces are absorbed by the black layer and do not contribute to the measurement which explains the missing red-shift in spectrum (V). A similar peak emission wavelength shift can be observed from configuration (IV) to (II).

Fig. 4 shows the internal optical efficiency  $\theta$ , the escape cone losses  $\kappa$  and the non-unity quantum yield losses  $\delta$  for all LSC designs in Table 1. The experimental results are derived using Eqs. (3) and (4) – standard method – or Eqs. (6) and (7) – simplified method. Experimental results match ray tracing simulations very closely confirming that our proposed experimental method accurately predicts the efficiency and loss channels of LSCs. For the ray tracing simulations the quantum yields stated in Table 1 are used for the respective concentrations; for concentrations in-between the quantum yield is linearly interpolated. The experimental results are represented via two error bars: the first error bar covers the internal optical efficiency of the three independent

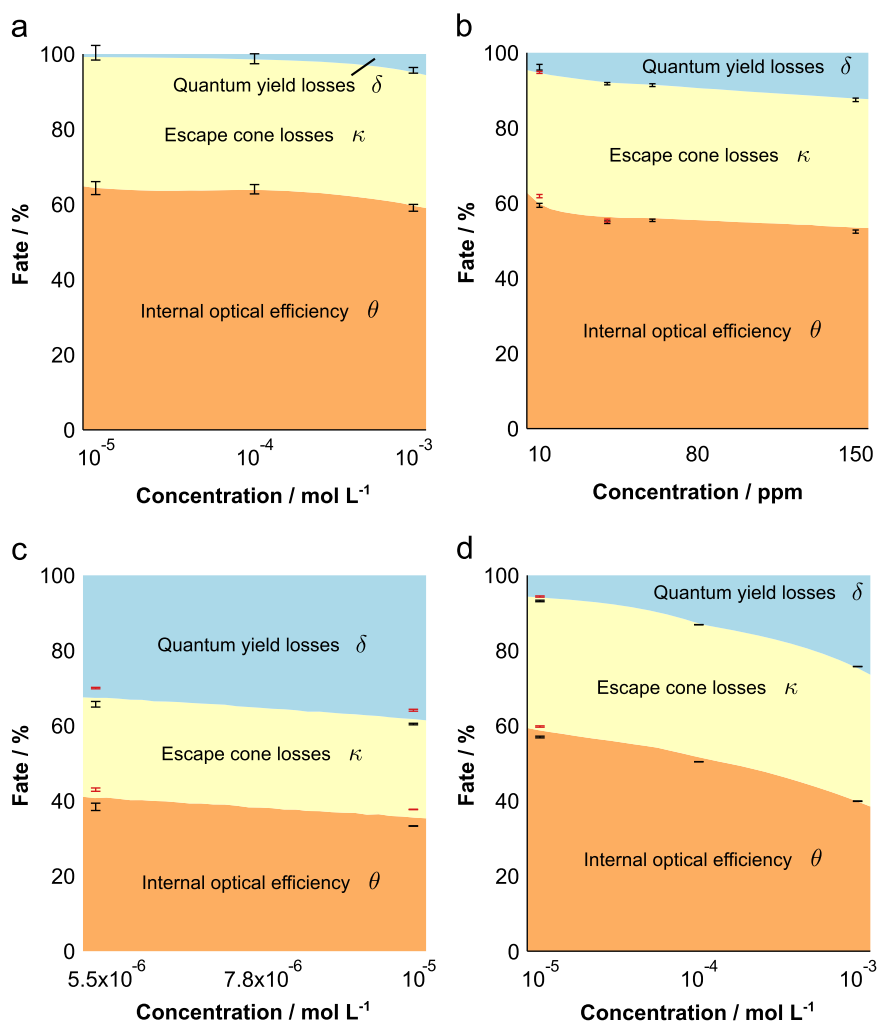


**Fig. 4.** Comparison between the experimental measurements (error bars) and ray tracing results (area plot) for all LSCs as a function of concentration. The results are shown for (a) Coumarin 6, (b) Lumogen R305, (c) Rhodamine 6G, and (d) Pyrromethene 567. The area plot depicts the fate of the photons once they have been absorbed: photons are either (1) concentrated to the side surfaces ( $\theta$  orange), (2) lost via the escape cone through the front and back surfaces ( $\kappa$  pale yellow), or (3) lost due to a non-unity quantum yield ( $\delta$  light blue). The lower error bar at each concentration represents the internal optical efficiency measured (for each LSC 3 measurements were taken). The higher error bar depicts the sum of the internal optical efficiency and escape cone losses. The experimental measurements using the standard method and the simplified method are shown using black and red error bars respectively. If both methods match very closely only the black error bars are shown. (For interpretation of the references to color in this figure caption, the reader is referred to the web version of this paper.)

measurements for each LSC and the second error bar covers the sum of the internal optical efficiency and the escape cone losses. Since the quantum yield losses are assumed to be unity minus the other loss channels, there is no need for a third error bar.

The metrics are quite stable ( $\theta \sim 64\%$ ,  $\kappa \sim 35\%$ ,  $\delta \sim 1\%$ ) for Coumarin 6 from  $10^{-5}$  mol L $^{-1}$  until  $10^{-4}$  mol L $^{-1}$  as re-absorption is limited at such concentrations and the quantum yield is very similar. Losses become slightly more dominant for the  $10^{-3}$  mol L $^{-1}$  concentration as the quantum yield is marginally lower ( $\theta \sim 59\%$ ,  $\kappa \sim 36.5\%$ ,  $\delta \sim 4.5\%$ ); additionally, the peak emission wavelength is red-shifted by 11.6 nm compared to the  $10^{-4}$  mol L $^{-1}$  sample. This indicates stronger re-absorption which aggravates escape cone and non-unity quantum yield losses. The error bars for the Coumarin 6 sample are slightly wider than for the other dye molecules as Coumarin 6 is emitting furthest to the blue part of the spectrum. The excitation source, a quartz tungsten halogen lamp, becomes weaker and the CCD spectrometer's sensitivity decreases towards the blue. As a result, the integration time of the spectrometer needs to be increased which lowers the signal-to-noise ratio.

For Lumogen R305 the internal optical efficiency decreases from  $\sim 59.5\%$  to  $\sim 52.5\%$  while increasing the concentration from 10 ppm to 150 ppm. While escape cone losses account for the

larger share of the total loss ( $\sim 36\%$  at all concentrations), the non-unity quantum yield losses make up for the lowering internal optical efficiency by increasing from  $\sim 4\%$  to  $\sim 12.5\%$ . It was shown previously that escape cone losses of LSCs doped with Lumogen R305 are independent of concentration and around 40% which matches our results closely [33].

Due to the lower quantum yield, Rhodamine 6G doped LSCs depict a substantially lower internal optical efficiency than Coumarin 6 or Lumogen R305 doped LSCs (standard method  $\sim 38.4\%$  and simplified method  $\sim 43\%$  at  $5.5 \times 10^{-6}$  mol L $^{-1}$  and standard method  $\sim 33.3\%$  and simplified method  $\sim 37.7\%$  at  $10^{-5}$  mol L $^{-1}$ ). Non-unity quantum yield losses are not only the main contributor to a decreasing internal optical efficiency but also exceed escape cone losses starting from the lowest concentration.

The internal optical efficiency of the Pyrromethene 567 LSCs drops off stronger with concentration than the Coumarin 6 LSCs. At a concentration of  $10^{-5}$  mol L $^{-1}$  the internal optical efficiency is measured to be around 57% which is comparable to the value achieved by the Coumarin 6 sample. However, the internal optical efficiency decreases to  $\sim 39.9\%$  at a concentration of  $10^{-3}$  mol L $^{-1}$  compared to  $\sim 59\%$  for Coumarin 6. This is partly due to the

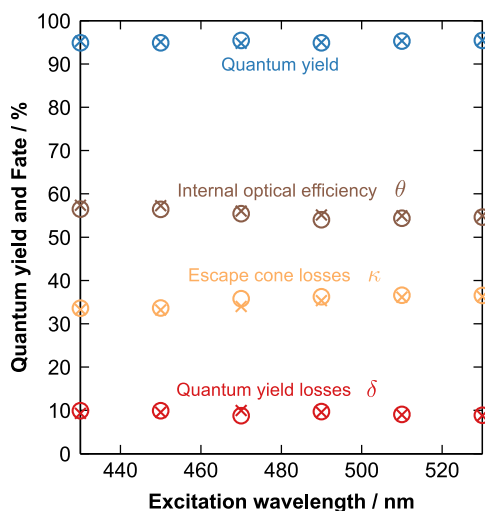


**Fig. 5.** Dependence of quantum yield (blue), internal optical efficiency (brown), escape cone losses (orange) and non-unity quantum yield losses (red) on excitation wavelength. Comparison between the standard (circles) and the simplified methods (crosses). (For interpretation of the references to color in this figure caption, the reader is referred to the web version of this paper.)

quantum yield of Pyrromethene 567 being slightly lower than the one of Coumarin 6; additionally, the Stokes shift of Pyrromethene 567 (14 nm) is less than half than the one of Coumarin 6 (35 nm) which will aggravate re-absorption, in particular at higher concentrations.

To demonstrate that the internal optical efficiency is independent of the incoming beam's wavelength, we varied the wavelength at which the incoming beam has its peak intensity. The LSC doped with Lumogen R305 at a concentration of 60 ppm was used for this measurement and the incoming wavelength was varied from 430 nm till 530 nm in 20 nm steps. The FWHM of the incoming beam was set to 10 nm to minimize the spectral overlap of the different incoming beams. Fig. 5 shows the measured quantum yield and LSC metrics as a function of incident wavelength. The quantum yield and the three LSC metrics remain stable while varying the wavelength of the incoming beam. Additionally, both methods agree very well.

Commonly, a solar cell is attached to only one side of the LSC instead of all four sides to limit the usage of expensive solar cell material [34–36]. In this case, one is interested in the share of photons reaching a particular side of the LSC. Our method has to be adjusted only slightly to account for that. In configurations (IV) and (V) only one side of the LSC should be covered with black marker; otherwise the measurements and calculations remain the same. Similarly, one can determine the share of photons reaching two or three sides. Fig. 6 shows the performance of the three Pyrromethene 567 LSCs with one, two, three and all four sides covered. Using a ternary plot, it becomes even more evident that the additional losses incurred due to a higher concentration are mostly due to non-unity quantum yield losses. Using fewer side surfaces though will almost exclusively aggravate escape cone losses. If a side surface is not covered with black marker, some of the photons previously being absorbed by the black marker – and thus considered to have reached the side surface/solar cell – will now leave the LSC through the side surface. Even though the photons leave the LSC via the side surface they contribute to escape cone losses as this particular side surface is not blackened and thus is not considered to have a solar cell attached.

As described in Section 2.3, once the internal optical efficiency and the loss probabilities have been measured relative to all absorbed photons for a LSC, the performance of the LSC relative to

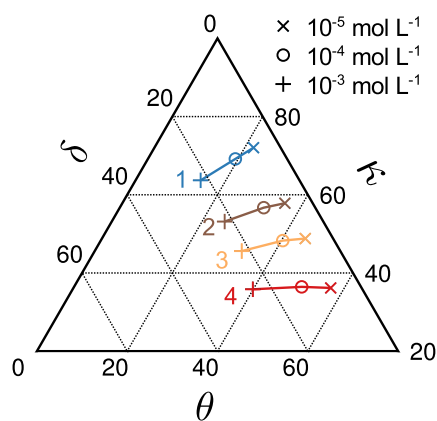


**Fig. 6.** Ternary plot showing the internal optical efficiency ( $\theta$ ), escape cone losses ( $\kappa$ ) and non-unity quantum yield losses ( $\delta$ ) for Pyrromethene 567 doped LSCs at concentrations of  $10^{-5}$  mol L<sup>-1</sup> (crosses),  $10^{-4}$  mol L<sup>-1</sup> (circles) and  $10^{-3}$  mol L<sup>-1</sup> (plus signs). Either one (blue), two (brown), three (orange), or four (red) side surfaces are blackened. (For interpretation of the references to color in this figure caption, the reader is referred to the web version of this paper.)

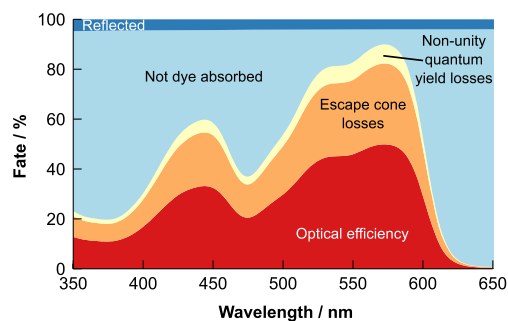


**Fig. 7.** Area plot showing the fate of photons relative to the number of incident photons for the Lumogen R305 LSC at 60 ppm. Photons can be reflected off the top surface (blue), not absorbed by a dye (light blue), lost due to a non-unity quantum yield (pale yellow), absorbed and re-emitted by a dye molecule but lost via the escape cone (orange), or concentrated towards the side surfaces (red). (For interpretation of the references to color in this figure caption, the reader is referred to the web version of this paper.)

all incident photons can be determined using Eq. (8) and an absorbance measurement of the LSC. Fig. 7 depicts the fate of incoming photons as a function of wavelength for the Lumogen R305 LSC at 60 ppm. The photons are either (1) reflected off the front surface, (2) not absorbed by a fluorophore, (3a) absorbed and lost due to a non-unity quantum yield, (3b) absorbed and lost due to escape cone losses, or (3c) absorbed and concentrated towards one of the side surfaces. Unlike the internal optical efficiency, the optical efficiency of a LSC is dependent on wavelength as it is a function of the absorption cross section of the fluorophore.

## 5. Conclusion

We have presented a novel method to measure the performance and the loss mechanisms of a LSC. The validity of our method is verified by comparing it with ray-tracing results which match the experimental findings closely. The method enables researchers for the very first time to clearly distinguish between escape cone losses and non-unity quantum yield losses which are the main loss channels for LSCs. We have also shown that our proposed metrics are independent of the incoming wavelength which reduces the number of required measurements significantly. By simply multiplying our metrics with the absorption

of the LSC, the response of the LSC over the entire wavelength spectrum of interest is derived.

If the equipment to measure the quantum yield of fluorophores in a solid sample is available, a research facility will find itself fully equipped to measure the optical efficiency and losses of LSCs. Therefore, our proposed method will have an immediate and positive impact on LSC research.

Recently, a new technique was proposed to measure the quantum yield of fluorophores that only requires two configurations [22]. In addition to presenting our experimental method, we have experimentally validated this new quantum yield measurement technique for the very first time by comparing the results to the most common technique to measure the quantum yield [20]. This finding is not only of importance for the field of LSCs but for researchers in various fields as quantum yield measurements are vital in multiple areas of science.

## Acknowledgments

This work was supported by the European Union Framework Programme 7 (FP7) via a Marie-Curie Career Integration Grant, Project no. 293567. We also acknowledge financial support from UCL BEAMS School via a Ph.D. Impact Award and from the UK Engineering and Physical Sciences Research Council (EPSRC grant no. EP/K015354/1). The authors would also like to thank Lucite International and BASF for supplying materials.

## Appendix A. Supplementary data

Supplementary data associated with this paper can be found in the online version at <http://dx.doi.org/10.1016/j.solmat.2015.08.008>.

## References

- [1] W.H. Weber, J. Lambe, Luminescent greenhouse collector for solar radiation, *Appl. Opt.* 15 (10) (1976) 2299–2300.
- [2] A. Goetzberger, W. Greube, Solar energy conversion with fluorescent collectors, *Appl. Phys.* 14 (2) (1977) 123–139.
- [3] P.P.C. Verbunt, A. Kaiser, K. Hermans, C.W.M. Bastiaansen, D.J. Broer, M.G. Debije, Controlling light emission in luminescent solar concentrators through use of dye molecules aligned in a planar manner by liquid crystals, *Adv. Funct. Mater.* 19 (17) (2009) 2714–2719.
- [4] N.C. Giebink, G.P. Wiederrecht, M.R. Wasielewski, Resonance-shifting to circumvent reabsorption loss in luminescent solar concentrators, *Nat. Photonics* 5 (11) (2011) 694–701.
- [5] C.S. Erickson, L.R. Bradshaw, S. McDowall, J.D. Gilbertson, D.R. Gamelin, D.L. Patrick, Zero-reabsorption doped-nanocrystal luminescent solar concentrators, *ACS Nano* 8 (4) (2014) 3461–3467.
- [6] W.E. Benjamin, D.R. Veit, M.J. Perkins, E. Bain, K. Scharnhorst, S. McDowall, D.L. Patrick, J.D. Gilbertson, Sterically engineered perylene dyes for high efficiency oriented fluorophore luminescent solar concentrators, *Chem. Mater.* 26 (3) (2014) 1291–1293.
- [7] M.G. Debije, C. Menelaou, L.M. Herz, A.P.H.J. Schenning, Combining positive and negative dichroic fluorophores for advanced light management in luminescent solar concentrators, *Adv. Opt. Mater.* 2 (7) (2014) 687–693.
- [8] M.J. Currie, J.K. Mapel, T.D. Heidel, S. Goffri, M.A. Baldo, High-efficiency organic solar concentrators for photovoltaics, *Science* 321 (5886) (2008) 226–228.
- [9] C.L. Mulder, L. Theogarajan, M. Currie, J.K. Mapel, M.A. Baldo, M. Vaughn, P. Willard, B.D. Bruce, M.W. Moss, C.E. McLain, J.P. Morseman, Luminescent solar concentrators employing phycobilisomes, *Adv. Mater.* 21 (31) (2009) 3181–3185.
- [10] C.L. Mulder, P.D. Reusswig, A.P. Beyler, H. Kim, C. Rotschild, M.A. Baldo, Dye alignment in luminescent solar concentrators: II. Horizontal alignment for energy harvesting in linear polarizers, *Opt. Express* 18 (S1) (2010) A91–A99.
- [11] C.L. Mulder, P.D. Reusswig, A.M. Velázquez, H. Kim, C. Rotschild, M.A. Baldo, Dye alignment in luminescent solar concentrators: I. Vertical alignment for improved waveguide coupling, *Opt. Express* 18 (S1) (2010) A79–A90.
- [12] C. Haines, M. Chen, K.P. Ghiggino, The effect of perylene diimide aggregation on the light collection efficiency of luminescent concentrators, *Sol. Energy Mater. Sol. Cells* 105 (2012) 287–292.
- [13] A. Menéndez-Velázquez, C.L. Mulder, N.J. Thompson, T.L. Andrew, P.D. Reusswig, C. Rotschild, M.A. Baldo, Light-recycling within electronic displays using deep red and near infrared photoluminescent polarizers, *Energy Environ. Sci.* 6 (1) (2013) 72–75.
- [14] A. Kerrouche, D.A. Hardy, D. Ross, B.S. Richards, Luminescent solar concentrators: from experimental validation of 3D ray-tracing simulations to coloured stained-glass windows for BIPV, *Sol. Energy Mater. Sol. Cells* 122 (2014) 99–106.
- [15] J.C. Goldschmidt, M. Peters, L. Prönneke, L. Steidl, R. Zentel, B. Bläsi, A. Gombert, S. Glunz, G. Willeke, U. Rau, Theoretical and experimental analysis of photonic structures for fluorescent concentrators with increased efficiencies, *Phys. Status Solidi* 205 (12) (2008) 2811–2821.
- [16] D.K.G. de Boer, D.J. Broer, M.G. Debije, W. Keur, A. Meijerink, C.R. Ronda, P.P.C. Verbunt, Progress in phosphors and filters for luminescent solar concentrators, *Opt. Express* 20 (S3) (2012) A395–A405.
- [17] C. Tummeltshammer, A. Taylor, A.J. Kenyon, I. Papakonstantinou, Homeotropic alignment and FRET: the way to a brighter luminescent solar concentrator, *J. Appl. Phys.* 116 (17) (2014) 173103.
- [18] R.W. MacQueen, T.W. Schmidt, Molecular polarization switching for improved light coupling in luminescent solar concentrators, *J. Phys. Chem. Lett.* 4 (17) (2013) 2874–2879.
- [19] J. ter Schiphorst, A.M. Kendhale, M.G. Debije, C. Menelaou, L.M. Herz, A.P.H.J. Schenning, Dichroic perylene bisimide triad displaying energy transfer in switchable luminescent solar concentrators, *Chem. Mater.* 26 (13) (2014) 3876–3878.
- [20] J.C. de Mello, H.F. Wittmann, R.H. Friend, An improved experimental determination of external photoluminescence quantum efficiency, *Adv. Mater.* 9 (3) (1997) 230–232.
- [21] J.R. Lakowicz, *Principles of Fluorescence Spectroscopy*, Springer, New York, NY, USA, 2006.
- [22] J. Valenta, Determination of absolute quantum yields of luminescing nanomaterials over a broad spectral range: from the integrating sphere theory to the correct methodology, *Nanosci. Methods* 3 (1) (2014) 11–27.
- [23] T.-S. Ahn, R.O. Al-Kaysi, A.M. Müller, K.M. Wentz, C.J. Bardeen, Self-absorption correction for solid-state photoluminescence quantum yields obtained from integrating sphere measurements, *Rev. Sci. Instrum.* 78 (8) (2007) 086105.
- [24] L.R. Wilson, B.C. Rowan, N. Robertson, O. Moudam, A.C. Jones, B.S. Richards, Characterization and reduction of reabsorption losses in luminescent solar concentrators, *Appl. Opt.* 49 (9) (2010) 1651–1661.
- [25] C. Tummeltshammer, M.S. Brown, A. Taylor, A.J. Kenyon, I. Papakonstantinou, Efficiency and loss mechanisms of plasmonic luminescent solar concentrators, *Opt. Express* 21 (S5) (2013) A735–A749.
- [26] W.G.J.H.M. van Sark, G.F.M.G. Hellenbrand, E.E. Bende, A.R. Burgers, L.H. Slooff, Annual energy yield of the fluorescent solar concentrator, in: 23rd European Photovoltaic Solar Energy Conference Exhibition, Valencia, Spain, 2008, pp. 198–202.
- [27] R. Reisfeld, G. Seybold, Stable solid-state tunable lasers in the visible, *J. Lumin.* 48 & 49 (1991) 898–900.
- [28] A. Kurian, N.A. George, B. Paul, V.P.N. Nampoore, C.P.G. Vallabhan, Studies on fluorescence efficiency and photodegradation of Rhodamine 6G doped PMMA using a dual beam thermal lens technique, *Laser Chem.* 20 (2002) 99–110.
- [29] G.A. Reynolds, K.H. Drexhage, New coumarin dyes with rigidized structure for flashlamp-pumped dye lasers, *Opt. Commun.* 13 (3) (1975) 222–225.
- [30] B.C. Rowan, L.R. Wilson, B.S. Richards, Advanced material concepts for luminescent solar concentrators, *IEEE J. Sel. Top. Quantum Electron.* 14 (5) (2008) 1312–1322.
- [31] J. Donovalová, M. Cigá, H. Stankovičová, J. Gašpar, M. Danko, A. Gáplovský, P. Hrdlovič, Spectral properties of substituted coumarins in solution and polymer matrices, *Molecules* 17 (2012) 3259–3276.
- [32] T.L. Arbeloa, F.L. Arbeloa, I.L. Arbeloa, I. Garca-Moreno, A. Costela, R. Sastre, F. Amat-Guerri, Correlations between photophysics and lasing properties of dipyrromethene BF2 dyes in solution, *Chem. Phys. Lett.* 299 (3) (1999) 315–321.
- [33] M.G. Debije, P.P.C. Verbunt, B.C. Rowan, B.S. Richards, T.L. Hoeks, Measured surface loss from luminescent solar concentrator waveguides, *Appl. Opt.* 47 (36) (2008) 6763–6768.
- [34] V. Sholin, J.D. Olson, S.A. Carter, Semiconducting polymers and quantum dots in luminescent solar concentrators for solar energy harvesting, *J. Appl. Phys.* 101 (12) (2007) 123114.
- [35] J. Bomm, A. Büchtemann, A.J. Chatten, R. Bose, D.J. Farrell, N.L.A. Chan, Y. Xiao, L.H. Slooff, T. Meyer, A. Meyer, W.G.J.H.M. van Sark, R. Koole, Fabrication and full characterization of state-of-the-art quantum dot luminescent solar concentrators, *Sol. Energy Mater. Sol. Cells* 95 (8) (2011) 2087–2094.
- [36] G.V. Shcherbatyuk, R.H. Inman, C. Wang, R. Winston, S. Ghosh, Viability of using near infrared PbS quantum dots as active materials in luminescent solar concentrators, *Appl. Phys. Lett.* 96 (19) (2010) 191901.